Recent progress in high-resolution magnetic imaging using scanning probe techniques

1999 J. Phys.: Condens. Matter 11 9387

(http://iopscience.iop.org/0953-8984/11/48/304)

J. Phys.: Condens. Matter **11** (1999) 9387–9402. Printed in the UK PII: S0953-8984(99)05147-4

Recent progress in high-resolution magnetic imaging using scanning probe techniques

M Bode†, M Dreyer, M Getzlaff, M Kleiber, A Wadas and R Wiesendanger

Institute of Applied Physics and Microstructure Research Centre, University of Hamburg, Jungiusstrasse 11, D-20355 Hamburg, Germany

E-mail: bode@physnet.uni-hamburg.de

Received 14 June 1999

Abstract. We have applied magnetic force microscopy (MFM) and spin-polarized scanning tunnelling spectroscopy (SP-STS) in ultrahigh vacuum (UHV) to study the magnetic domain structure of Co/Au(111) and Gd/W(110), respectively. A new measurement mode will be presented which minimizes possible accidental interactions between the probe tip and the sample in UHV-MFM. This allows the investigation of the well known spin reorientation transition of Co films grown on Au(111) at nanometre-scale spatial resolution. Details of domain walls and the domain structure as a function of CO coverage are studied. Spin-polarized tunnelling is realized by using an Fe-coated W tip and a sample which exhibits an exchange-split surface state. Magnetic domain imaging with a spatial resolution below 20 nm is demonstrated for Gd/W(110). The observed bias dependent spin polarization of Gd(0001) is in good agreement with spin-resolved inverse photoemission spectroscopy results.

1. Introduction

Due to the rapidly increasing storage density of magnetic disks and tapes high-resolution imaging of magnetic domain structures is of considerable economic as well as scientific interest. Conventional magnetically sensitive techniques, however, offer either poor spatial resolution which is limited by the wavelength of light used as in the case of conventional optical microscopy with polarization analysis, or suffer from other drawbacks like the destructive nature of the Bitter technique. Since the invention of the scanning tunnelling microscope (STM) [1] as the prototype of near-field techniques several related scanning probe methods with the ability to image magnetic domains have been developed [2].

Here, we report on our recent progress in magnetic force microscopy (MFM) and spin-polarized scanning tunnelling spectroscopy (SP-STS). In MFM the magnetic stray field of the sample is probed by a magnetically covered pyramidal tip brought very close to the sample surface. Since the tip is integrated in a microfabricated cantilever the dipole–dipole force between the tip and the sample can be measured by detecting the bending of the cantilever by means of beam deflection. Alternatively, the force gradient can be determined by oscillating the cantilever and measuring the frequency shift within the stray field compared to the freely oscillating cantilever. Although the spatial resolution which can be achieved with MFM strongly depends on the minimal tip–sample distance, typically a resolution well below 100 nm is obtained.

† Corresponding author.

0953-8984/99/489387+16$30.00

One mode of operation often used to image the magnetic domain structure of a sample with the MFM under ambient conditions is the so-called lift mode. In this mode every line is scanned twice: first, the topography is measured with tip and sample in contact. Then the feedback is switched off and the tip is moved along the contour of the topography keeping the tip–sample distance constant at several tens of nm. In the second scan only the long-range dipole–dipole interactions between the magnetic probe tip and the magnetic sample contribute to the force signal. However, any thin interface layer present under ambient conditions between the sample and the tip changes the overall tip–sample interaction potential in a undefined manner. This layer consists mainly of water with some other molecules like hydrocarbons from the air. Moreover, the oxidization process might influence the magnetic sample and the thin film MFM tip while running MFM in air. Covering the sample by a protection layer does not help, since the layer itself may influence the magnetic structure especially of a thin film sample [3]. Finally, the frequent contact between tip and sample may lead to a destructive interaction, i.e. an accidental manipulation of the sample domain structure.

Ultrahigh vacuum (UHV) provides conditions to study magnetic materials by MFM without any non-magnetic layer between the sample and the probing tip. Applying MFM under UHV conditions leads to some additional advantages. Since neither the magnetic probe tip nor the sample needs to be protected against oxidation the effective tip to sample distance is reduced leading to an improved spatial resolution. Furthermore, when measuring force gradients the sensitivity is enhanced. Unfortunately, due to adhesion forces which remain present the application of magnetic force microscopy under UHV conditions is not straightforward. In order to overcome this obstacle we have developed a new measurement mode that minimizes the contact between tip and sample and allows the imaging of the domain structure of Co/Au(111) in the vicinity of the spin reorientation transition.

Nowadays, the use of topographic and spectroscopic modes of the scanning tunnelling microscope (STM) almost routinely allows the correlation of local structural with electronic properties down to the atomic scale. It is an obvious idea to make the STM sensitive to the spin of the tunnelling electrons by using a magnetic probe tip. The basic working principle is well known as the *spin-valve effect* [4]: since ferromagnetic materials exhibit a spin imbalance at the Fermi level E_F and the electron spin has to be preserved in an elastic tunnelling process the conductivity of a tunnelling junction *must* depend on the relative magnetization direction between tip and sample. Pioneering experiments on spin-polarized tunnelling in ferromagnet–insulator–superconductor planar junctions have been performed by Tedrow *et al* [5, 6]. In 1975, Julliere [7] proved that spin-polarized tunnelling can also be realized between two ferromagnetic electrodes. The application of spin-polarized tunnelling in a new generation of random access memory (RAM) devices, the so-called magnetic RAM (MRAM), is intensively discussed in [8].

In spite of the progress made with planar devices there are only few experiments which report on the observation of a spin-dependent tunnelling current using an STM [9, 10]. Probably, this is caused by one important difference between planar tunnelling junctions and the STM: while the electrodes of a planar junction are rigidly connected by the insulating barrier the setup of a STM is much less rigid since it must necessarily include positioning devices which allow movement of the probe tip relative to the sample. This certainly leads to a higher noise level in the STM than in the planar setup which might mask such tiny effects as those expected in the case of spin-polarized tunnelling. Our experimental approach to overcome these difficulties is based on tunnelling into the well known surface state of Gd(0001) which is exchange split into a filled majority and an empty minority spin contribution [11, 12]. Therefore, we are able to use *two* spin-polarized electronic states with *opposite* polarization to probe the magnetic orientation of the sample relative to the tip. In other words, we perform

a single experiment that simultaneously measures the spin-valve effect acting differently on the two spin components of Gd(0001). This reduces the influence of tip changes and slight fluctuations of the tip–sample distance.

2. Magnetic force microscopy under ultrahigh-vacuum conditions

The development of a new measurement technique requires a suitable test sample that allows demonstration of the abilities and restrictions of this technique. Ultrathin Co films grown on Au(111) are ideally suited for this purpose since this system exhibits a well known magnetic reorientation transition from out-of-plane to in-plane anisotropy at a thickness between 3 and 5 monolayers (ML) which has previously been studied by scanning electron microscopy with polarization analysis (SEMPA) [13, 14]. Indeed, for clean Co/Au(111) our MFM observations of the magnetic reorientation transition are in full agreement with earlier SEMPA studies. Furthermore, the high sensitivity and spatial resolution of UHV-MFM allows imaging of the magnetic domain structure for a Co coverage as low as 1.8 ML. We found that the presence of carbon can significantly delay the critical thickness of the reorientation transition by at least a factor of four. This surprising result may have applications using ultrathin carbon-containing Co films for high-resolution perpendicular magnetic recording [15].

2.1. Experimental details

To measure force gradients the cantilever is vibrated at its resonance frequency $\omega = \sqrt{k_{\mathrm{eff}}/m}$, where m denotes the mass of the cantilever and k_{eff} the effective spring constant. The latter is given by $k_{\mathrm{eff}} = k - F'$, where F' is the overall force gradient acting on the cantilever and k is the nominal spring constant of the cantilever. The change in the force gradient while scanning over the surface shifts the resonance frequency ω. In our system the shift due to magnetic tip–sample interaction is measured with a frequency modulation (FM) detector. The lowest detectable force can be estimated according to [16]:

$$F_{\mathrm{min}} = \frac{1}{A}\sqrt{\frac{4kk_{\mathrm{B}}TB}{\omega_0 Q}} \tag{1}$$

where A denotes the rms amplitude of the oscillation, B the detection bandwidth and Q the quality factor of the oscillator. Since the Q-factor of the cantilever is increased due to the absence of air damping the sensitivity is increased when measuring in UHV.

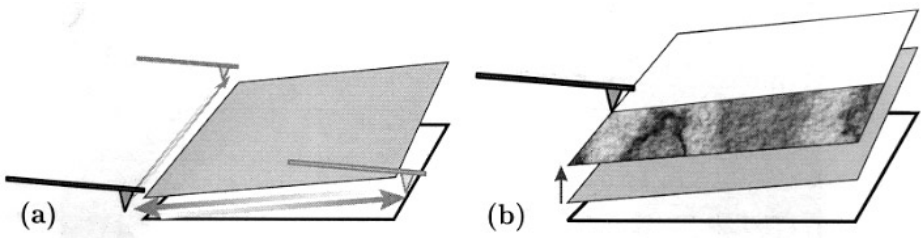

Figure 1. Schematic view of the *plane subtraction mode*. (a) First the sample is scanned several times along two or four sides of an area larger than the region of interest. The scan lines of each side are averaged and a polygon of given order is fitted to each of the averaged lines. (b) The parameters are used to estimate the position of the sample in 3D space and thus to keep the tip at the given distance from the sample.

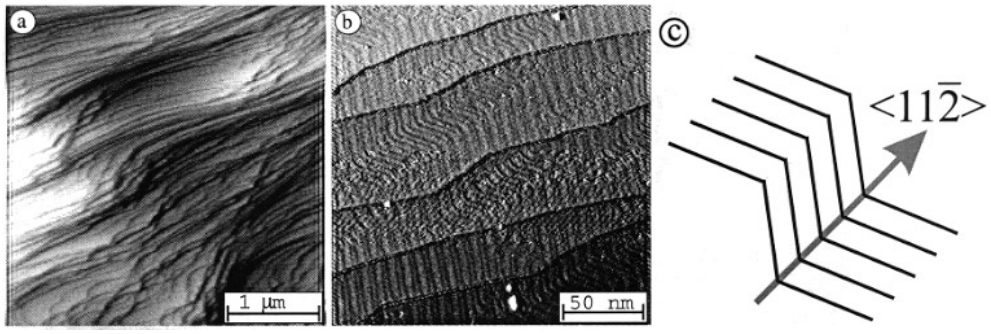

Figure 2. (a) Step bunches along the [11$\bar{2}$]-direction can be recognized in the large-scale STM image of the clean Au(111) surface. (b) The (23 × $\sqrt{3}$) *herringbone* reconstruction appears in images with a smaller scan range. (c) The relative orientation between the crystal lattice and the reconstruction.

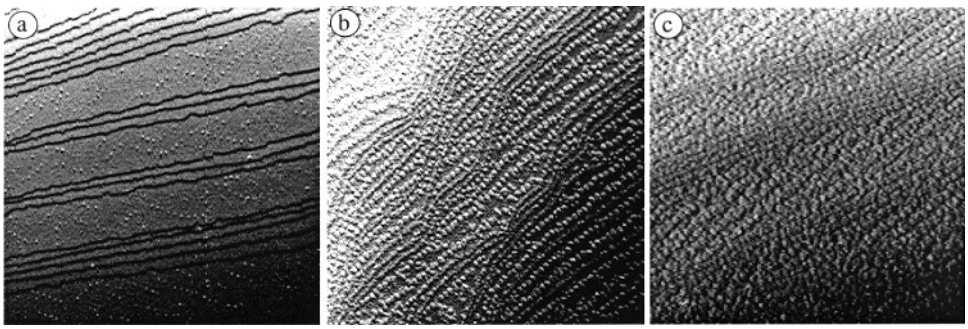

Figure 3. STM images showing the growth of Co/Au(111) at coverages of (a) 0.07 ML, (b) 0.5 ML and (c) 4 ML. In the early stage Co islands of a height of two monolayers decorate the elbow sites of the underlying Au(111) *herringbone* reconstruction thereby forming rows of islands along the [11$\bar{2}$]-direction of the substrate (scan range: 400 nm × 400 nm).

In order to minimize the tip–sample interaction we implemented the so-called plane subtraction mode (PS mode) [17]. In our setup the sample is scanned in the contact mode, i.e. without any modulation of the cantilever, only along two or four sides of an area larger than the region to be scanned in MFM mode (figure 1(a)). Then a polynomial of given order is fitted to the data. The coefficients are used to extrapolate the height of the sample at each point inside the region of interest. Then the feedback loop is switched off and the tip is retracted by about 100 nm. This guarantees overcoming the strong adhesion interaction between tip and sample even when using a soft cantilever. At this height the oscillation of the cantilever (amplitude ≈10 nm) is switched on. Finally, the tip is lowered to the final tip–sample separation of typically 20–40 nm at which the sample will be scanned (figure 1(b)).

The MFM sensors were prepared by depositing iron films in the UHV chamber on commercially available Si cantilevers with integrated tips. Typically, we used a spring constant of 1–4 N m^{-1} and a resonance frequency of 60–80 kHz. First, the cantilevers were cleaned by Ar^+-ion etching (90 min, $E_{ion} = 1.5$ keV). Subsequently, we have used electron beam evaporation in order to deposit about 20 nm Fe upon the tips. We used a single crystalline Au substrate with miscut lower than 2° towards the (111)-plane. The crystal was prepared by cycles of Ar^+-ion etching at an ion energy of 600 eV and heating to 450 °C resulting in

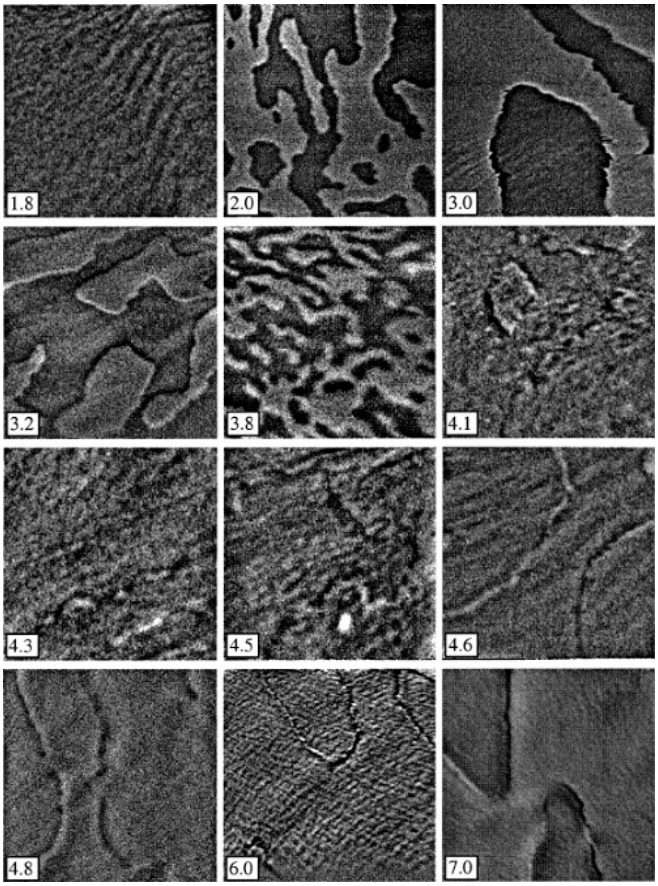

Figure 4. MFM images obtained at increasing Co film thicknesses. The numbers denote the actual film thickness in monolayers. Scan size: 5 μm $\times$ 5 μm.

a clean Au(111) surface that exhibits the well known $(23 \times \sqrt{3})$ reconstruction [18]. The topography of the clean Au(111) surface as measured in the constant-current STM mode is shown in figure 2. For calibrating the Co evaporator, we prepared a sub-monolayer film on the Au(111) single crystal and measured the actual coverage by STM to obtain the evaporation rate (figures 3(a) and (b)). Co starts growing in islands of 2 ML at the elbow sites of the $(23 \times \sqrt{3})$ reconstruction [19].

2.2. Results

Figure 4 shows MFM data of the coverage dependent domain structure of Co/Au(111) using several different cantilevers with the magnetization pointing roughly along the tip axis. Already at a Co coverage Θ as low as 1.8 ML a weak contrast is visible, which will be discussed later. For 2.0 ML $\leqslant \Theta \leqslant$ 3.8 ML areas with a strong dark and bright contrast appear originating from magnetic domains of a film magnetized perpendicular to the surface. Obviously, the domain size first increases with increasing coverage with a maximum at $\Theta = 3$ ML but then decreases between 3.2 and 3.8 ML. This result is in full agreement with SEMPA measurements [14]. For the next three images, which represent a Co film thickness of 4.1, 4.3 and 4.5 ML respectively,

blurred dark and bright lines roughly along the [11$\bar{2}$]-direction can be recognized. In this coverage range the easy axis of the Co film rotates from out of plane to in plane and magnetically the sample is extremely soft [13, 14]. For this particular coverage we cannot exclude that the sample domain structure is manipulated by the stray field of the MFM tip. The contrast becomes more clear at $\Theta \geqslant 4.6$ ML. It now originates from domain walls which appear as lines with different black/white segments. The signal fluctuation within the magnetic domains can be interpreted as a magnetic ripple structure [20, 21].

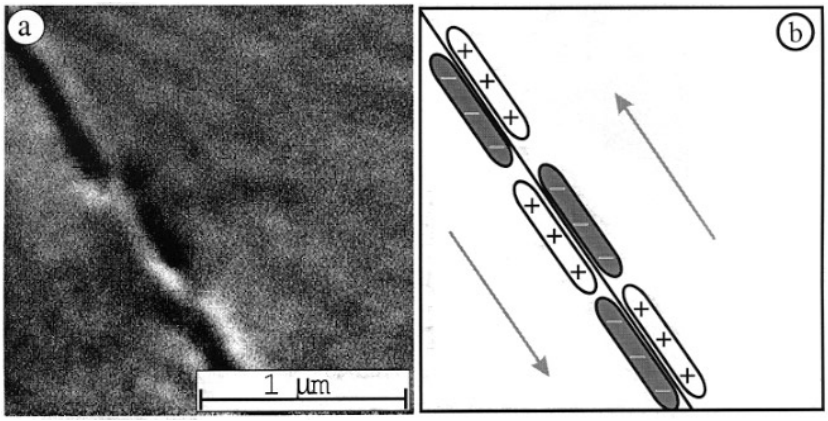

Figure 5. (a) Detail of a domain wall measured in the PS mode on 11.5 ML Co/Au(111). Along the domain wall the contrast reverses twice. (b) Schematic representation of the magnetic domains (arrows) and the magnetic charges (+, −) which are caused by different rotation directions within the Néel wall.

The high spatial resolution of MFM allows a more detailed characterization of the domain walls that appear in Co films with an in-plane magnetization. Figure 5(a) shows an MFM image of 11.5 ML Co/Au(111). A domain wall crossing the imaged area appears as parallel dark and bright stripes. Two contrast reversals occur within the scanned frame. Schematically, the domain structure is shown in figure 5(b). Two domains with opposite magnetizations (grey arrows) are separated by a 180° domain wall (black line). It has been theoretically proposed [22] that Néel walls preferentially occur in magnetic films with a thickness below 40 nm, i.e. the magnetization rotates within the film plane. This rotation leads to uncompensated magnetic dipoles within the Néel wall which cause magnetic surface charges, + on one side and − on the other side. The charges increase or decrease the measured force gradient, respectively. However, the rotation might occur either clockwise or anticlockwise. As a consequence the domain wall contrast as observed in figure 5(a) can be explained by a Néel wall that changes rotation direction twice.

In previous SEMPA experiments ferromagnetic order could be observed for Co coverages as low as 2.0 ML. By means of MFM, however, we obtained a magnetic signal for Co coverages as low as 1.8 ML (cf figure 4). Figures 6(a) and (b) show STM data with a scan range of 400 nm × 400 nm and 100 nm × 100 nm, respectively. The Co film consists of islands of 2 ML height, on which the third and fourth layer have already started to grow. The islands began to coalesce mainly at the step edges of the substrate, but there are still single islands as well as fractions of uncovered Au. Two MFM images of 3 μm × 3 μm and 1.5 μm × 1.5 μm scan area are displayed in figure 6(c) and (d). In the upper right corner of image 6(d), image (a) is displayed at the same scale as image (d) for comparing the sizes of the magnetic and topographic features. The MFM images reveal bright and dark stripes of about 50–100 nm

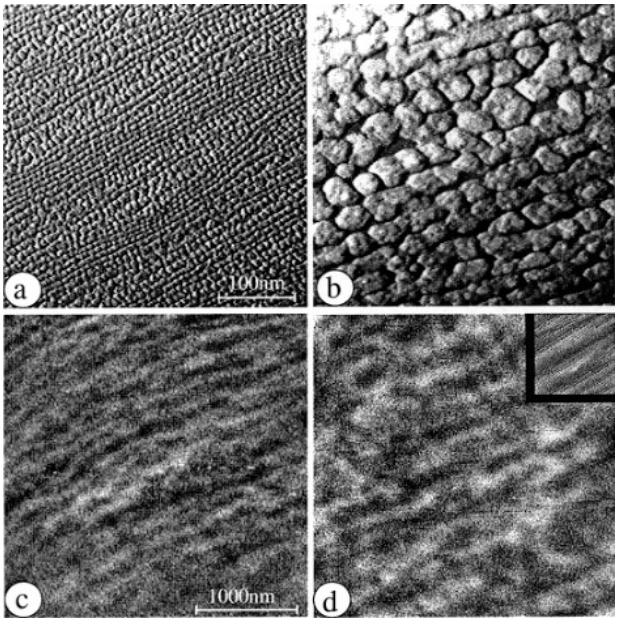

Figure 6. STM and MFM images of a Co film of 1.8 ML thickness. The images (a) and (b) show STM data of 400 nm × 400 nm and 100 nm × 100 nm scan size. Images (c) and (d) display MFM data of the same sample of 3 μm × 3 μm and 1.5 μm × 1.5 μm scan size. For comparison, image (a) is displayed as an inset in image (d) at the same scale.

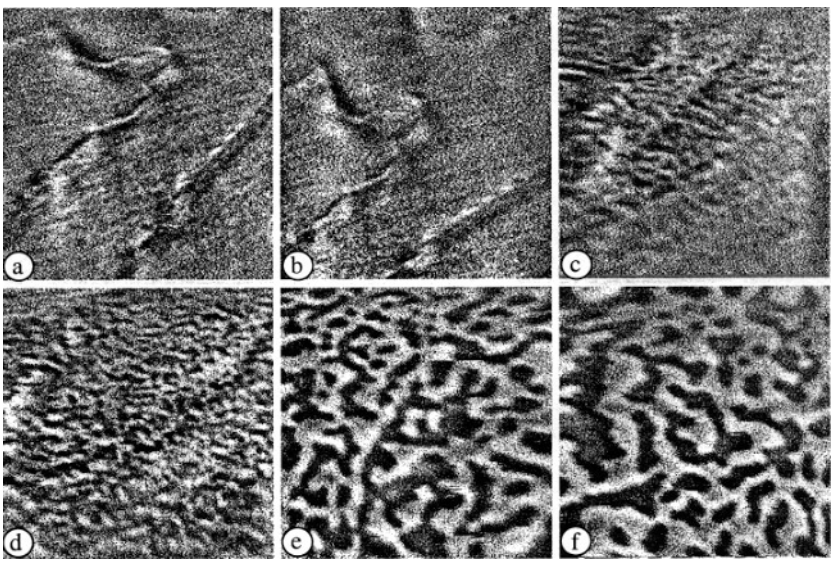

Figure 7. Evolution in time of the magnetic structure of a 5 ML Co film due to C contamination. The images were taken about 2, 6, 7, 8, 8.2 and 13 days after the sample preparation (scan range 5 μm × 5 μm).

width, running mainly from the bottom left to the upper right corner, i.e. along the steps of the Au(111) crystal.

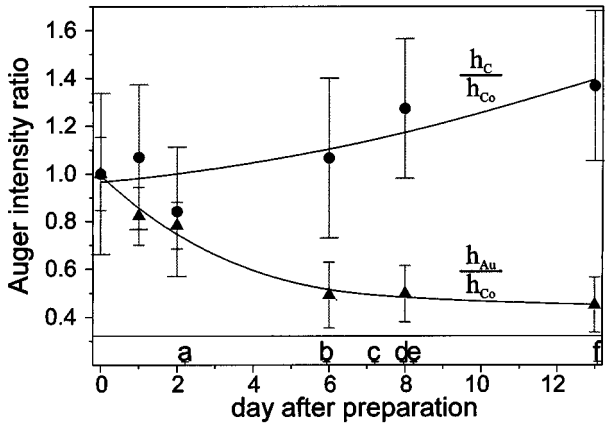

Figure 8. Intensity of the C(272) and Au(165) Auger line with respect to the intensity of the Co(656) Auger line plotted against time for the 5 ML Co film (letters a–f correspond to the MFM images in figure 7).

The observation of the same Co film for a longer period of time reveals a change of its magnetic structure. Figure 7 shows a series of MFM images measured on one particular 5 ML thick Co film grown on Au(111) at different time intervals after preparation. As already shown in figure 4 at this particular Co coverage the easy magnetization direction of a clean film is in plane. Indeed, the contrast of figure 7(a) which was measured 2 days after preparation is dominated by parallel dark and bright lines which represent Néel walls and the magnetic ripple structure. The MFM images shown in figures 7(b)–(f) were measured on the same sample 6, 7, 8, 8.2 and 13 days after preparation. Already in figure 7(c) small perpendicular domains are visible, which become more pronounced in figure 7(d). Obviously, the perpendicular domains increase in size with time that elapses since the sample preparation (cf figures 7(e) and (f)). Former work indicates two possible reasons for this change. Firstly, Speckmann *et al* showed that annealing Co/Au(111) shifts the critical thickness of the reorientation transition caused by the migration of Au onto the sample surface [14]. Secondly, Hope *et al* revealed that the easy axis of magnetization of Co/Cu(110) can be switched by 90° from in plane to out of plane by means of CO dosing [23]. We have performed Auger electron spectroscopy (AES) in order to check whether the first or second mechanism leads to the rotation of the easy magnetization in our case. From the AES data the peak heights of two Auger lines, Au(165) (h_{Au}) and Co(656) (h_{Co}), were extracted. The quotient $h_{\mathrm{Au}}/h_{\mathrm{Co}}$ is plotted versus time in figure 8. Each data point represents the average of five consecutively measured Auger spectra. If Au migrated onto the sample surface the $h_{\mathrm{Au}}/h_{\mathrm{Co}}$-ratio should rise in time, which can be clearly excluded on the basis of the data. In contrast, the increasing C(272) Auger peak height relative to the Co(656) peak height, i.e. ($h_{\mathrm{C}}/h_{\mathrm{Co}}$), indicates a progressive C contamination of the Co film probably caused by the dissociative adsorption of CO present in the residual gas of the UHV system.

3. Spin-polarized scannning tunnelling spectroscopy

To realize spin-polarized tunnelling by using an STM the difficult problem of separating topographic, electronic and magnetic information has to be solved. Our experimental approach to overcome these difficulties is based on tunnelling into the well known surface state of

Gd(0001) which is exchange split into a filled majority and an empty minority spin contribution [11, 12]. In analogy to the low-temperature experiments performed with ferromagnet–insulator–superconductor planar tunnelling junctions [5, 6] where the quasiparticle density of states of superconducting aluminium is split by a magnetic field into spin-up and spin-down parts, we use two exchange-split electronic states with opposite polarization to probe the magnetic orientation of the sample relative to the tip. We demonstrate spin-polarized tunnelling by measuring the asymmetry of the differential tunnelling conductivity at bias voltages corresponding to the energetic positions of the two spin contributions of the exchange-split surface state in an external magnetic field. This enables the electronic and magnetic structure information to be clearly separated.

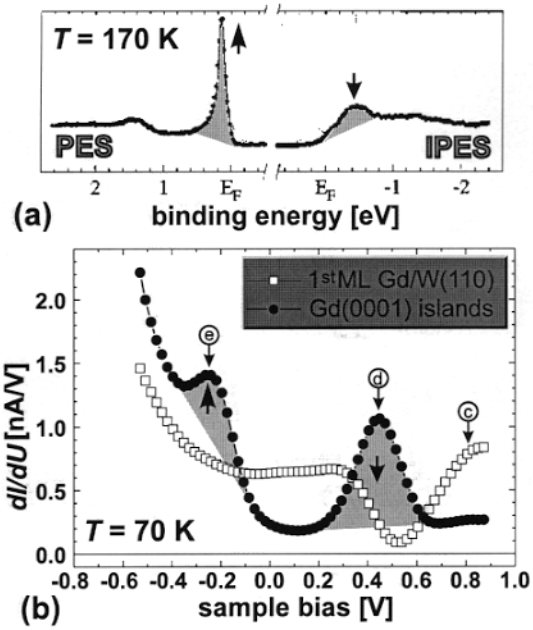

Figure 9. (a) Photoemission (left) and inverse photoemission (right) spectra of Gd(0001) measured at 170 K (from Weschke *et al* [29]). The occupied part of the surface state appears in the PE spectrum while the empty part is weakly visible in the IPE spectrum. (b) Tunnelling spectrum measured above a Gd(0001) island and above the first distorted ML at 70 K. Spatially resolved data at sample bias values indicates by small arrows (c)–(e) will be shown in figure 10.

3.1. The Gd(0001) surface state

Gadolinium (Gd) has often been regarded as a prototype rare-earth metal since it exhibits a half-filled 4f shell which carries—according to Hund's rule—the maximal possible f-shell magnetic moment of 7 μ_B. Below the Curie temperature of 292.5 K Gd is ferromagnetic. The atomic 4f moments are exchange coupled via the Ruderman–Kittel–Kasuya–Yosida (RKKY) interaction mediated by the 5d-like conduction electrons which also give a small contribution to the total magnetic moment of about 0.6 μ_B. In 1991, Freeman and co-workers [24] proposed the existence of a highly localized d_{z^2}-like surface state on Gd(0001). According to this calculation the surface state is exchange split into an occupied majority and an empty minority branch. Indeed, the existence of the occupied majority part of the d_{z^2}-like surface state was

soon confirmed experimentally [25]. Later, also the empty minority part of the surface state was found by inverse photoemission (IPE) [26]. Although an antiferromagnetic (AFM) coupling has been proposed in the original contribution [24] it is nowadays accepted that the bulk and (0001) surface of Gd(0001) couple ferromagnetically (FM) [12, 27, 28].

It was a basic question in the framework of this study whether it is possible to observe the d_{z^2}-like Gd(0001) surface state by means of STS. Figure 9(a) shows photoemission (PES) and inverse photoemission spectroscopy (IPES) data of Gd(0001) measured at $T = 170$ K as published by Weschke *et al* [29]. While the PE measurement shows the occupied part of the surface state at a binding energy $E_{\mathrm{bin}} \approx 130$ meV the empty part appears in the IPE spectrum at $E_{\mathrm{bin}} \approx -420$ meV. It is a significant advantage of STS that it is sensitive to the local density of states (LDOS) on both sides of the Fermi level by tuning the applied bias voltage from negative to positive bias or vice-versa. Indeed, the $\mathrm{d}I/\mathrm{d}U$-spectrum measured with the tip positioned above a Gd(0001) island exhibits two distinct maxima at sample bias values of $U = -200$ mV and $U = +430$ mV (figure 9(b)), being in good agreement with the binding energies for the occupied and the empty part of the surface state as determined by PE and IPE (cf figure 9(a)). In contrast to the Gd(0001) islands the spectra measured above the monolayer exhibit only a single asymmetric peak at a positive sample bias $U = +300$ mV, i.e. in the empty sample states, which is of different origin.

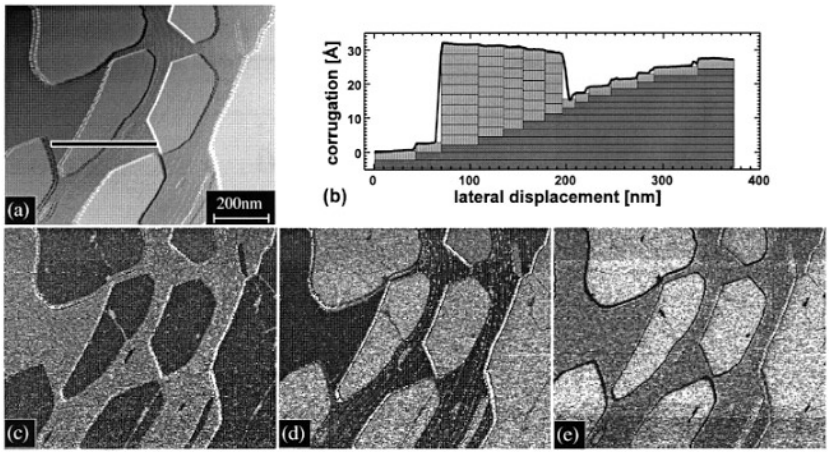

Figure 10. (a) Constant-current STM topograph of nominally 5 ML Gd(0001)/W(110). The substrate was held at 530 K during evaporation resulting in Stranski–Krastanov growth. (b) Line section extracted from (a). Maps of the differential conductivity $\mathrm{d}I/\mathrm{d}U$ measured at different sample bias are shown in (c) $U = +0.8$ V, (d) $U = +0.45$ V and (e) $U = -0.22$ V.

Figure 10(a) shows the topograhy of a sample prepared by deposition of 5 ML Gd/W(110) at 530 K resulting in Stranski–Krastanov growth, i.e. island formation. Several islands can be recognized that are atomically flat on top. Below the islands the substrate exhibits numerous monatomic steps. Therefore the coverage increases on going from the right to the left island edge as schematically indicated in the line section shown in figure 10(b). For this particular island we found local coverages of 6 ML $\leqslant \Theta_{\mathrm{loc}} \leqslant$ 10 ML. Simultaneously with the topography we have measured a $\mathrm{d}I/\mathrm{d}U$-spectrum at every pixel of the scan. During the measurement the sample was held at $T = 70$ K. Figures 10(c)–(e) show maps of the differential conductivity $\mathrm{d}I/\mathrm{d}U$ for different sample bias: (c) $U = +0.8$ V, (d) $U = +0.45$ V and (e) $U = -0.22$ V. These sample bias values have been marked by arrows in figure 9(b). The differential conductivity is grey coded, i.e. the higher the local $\mathrm{d}I/\mathrm{d}U$-signal the brighter

a location appears. At a sample bias of $U = +0.8$ V the tunnelling current is dominated by electrons which tunnel from the tip into unoccupied sample states with a binding energy of +0.8 eV. Comparison with the topographic data of figure 10(a) reveals that at this particular binding energy the differential conductivity above the Gd monolayer is higher than above any island. Beside a few small bright spots the $\mathrm{d}I/\mathrm{d}U$-signal at $U = +0.8$ V measured above the Gd islands is uniform†. At $U = +0.45$ V the contrast between the island surface and the monolayer is inverted. This sample bias corresponds to the binding energy of the empty Gd(0001) surface state (cf figure 9(b)). Qualitatively the same situation occurs at $U = -0.22$ V (figure 10(e)), i.e. at the energetical position of the occupied surface state. We never found a contrast in the $\mathrm{d}I/\mathrm{d}U$-maps on Gd islands with $\Theta_{\mathrm{loc}} \geqslant 10$ ML at any sample bias in the voltage range under study, i.e. -0.6 V $\leqslant U \leqslant +0.9$ V. We could show that only for a Gd coverage below 4 ML is the binding energy of the occupied part of the surface state reduced [32].

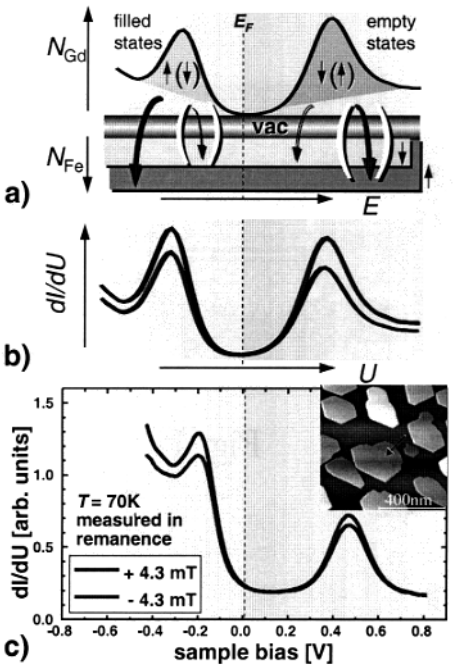

Figure 11. (a) The principle of SP-STS using a sample with an exchange-split surface state, e.g. Gd(0001), and a magnetic Fe tip with a constant spin polarization close to E_{F}: due to the spin-valve effect the tunnelling current of the surface state spin component, parallel to the tip, is enhanced at the expanse of its spin counterpart. (b) This should lead to a reversal in the $\mathrm{d}I/\mathrm{d}U$-signal at the surface state peak position upon switching the sample magnetically. (c) Exactly this behaviour could be observed in the tunnelling spectra measured with the tip positioned above an isolated Gd island (see arrow in the inset).

3.2. Spin-polarized tunnelling

As mentioned above our experimental approach towards spin-polarized tunnelling relies on the existence of an exchange-split surface state on the Gd(0001) surface [34]. The principle

† The bright spots reflect an increased LDOS at this particular sample bias which is induced by the local adsorption of hydrogen [30, 31]. The total amount of hydrogen adsorbed on the surface is below 0.01 L (1 Langmuir $= 1 \times 10^{-6}$ Torr s).

of spin-polarized scanning tunnelling spectroscopy (SP-STS) is schematically illustrated in figure 11. Since the majority (minority) part of the Gd(0001) surface state has a binding energy of −220 meV (500 meV) at 20 K, i.e. an exchange splitting $\Delta_{ex} \leqslant 700$ meV, both spin parts are relatively close to the Fermi level and therefore easily accessible by STS†. In the following we consider vacuum tunnelling between an exchange-split surface state and a tip material for which the sign of the spin polarization does not reverse in the energy range of interest, i.e. ±0.5 eV around the Fermi level. According to first-principles calculations this condition is fulfilled for Fe [35]. For simplicity a constant spin polarization‡ (figure 11(a) bottom) and a magnetization direction of the tip to be collinear with the sample magnetization are assumed. Since both the majority and the minority component of the Gd(0001) surface state appear in our tunnelling spectra, in any case the spins of *one* component of the surface state will be *parallel* with the majority spin of the tip while the *other one* will be *antiparallel*. Therefore, the spin-valve effect will act differently on the two spin components: the spin component of the surface state parallel to the majority spins of the tip is enhanced at the expense of its counterpart being antiparallel. Consequently, by comparing tunnelling $\mathrm{d}I/\mathrm{d}U$-spectra measured above domains with opposite magnetization we expect a reversal in the contrast at the majority and minority surface state peak position (figure 11(b)).

Indeed, tunnelling spectra measured in an external magnetic field with an Fe-coated probe tip ($\Theta_{tip} = 10$ ML) positioned above an isolated Gd(0001) island show exactly the expected behaviour (figure 11(c)). After inserting the sample in the STM sample holder and cooling down to 70 K it was magnetized in a magnetic field of +4.3 mT applied parallel to the sample surface. Subsequently, 128 tunnelling $\mathrm{d}I/\mathrm{d}U$-spectra were measured in remanence with the tip positioned above the Gd island marked by an arrow in the inset of figure 11(c). Then the direction of the magnetic field was reversed (−4.3 mT) and a further 128 tunnelling $\mathrm{d}I/\mathrm{d}U$-spectra were measured at the same location. This procedure was repeated several times. Figure 11(c) shows the averaged tunnelling spectra measured in remanence after the application of a positive or negative field. Comparison of the spectra reveals that for positive field the differential conductivity $\mathrm{d}I/\mathrm{d}U$ measured at a sample bias which corresponds to the binding energy of the occupied (majority) part of the surface state is higher than for negative field. The opposite is true for the empty (minority) part. We have chosen Gd islands on W(110) for this experiment since it is known from Kerr-effect measurements [36] that their coercivity is only 1–1.5 mT, i.e. much lower than the applied field. Therefore, one can safely conclude that the magnetization of the sample was switched by the external field while the tip magnetization remained unchanged.

The spin polarization of the tunnelling current can be estimated [38] by

$$P(U) \equiv \frac{\mathrm{d}I/\mathrm{d}U_{\uparrow}(U) - \mathrm{d}I/\mathrm{d}U_{\downarrow}(U)}{\mathrm{d}I/\mathrm{d}U_{\uparrow}(U) + \mathrm{d}I/\mathrm{d}U_{\downarrow}(U)} \tag{2}$$

where $\mathrm{d}I/\mathrm{d}U_{\uparrow(\downarrow)}(U)$ is the intensity of the $\mathrm{d}I/\mathrm{d}U$-signal measured with the sample remanently magnetized in opposite directions (↑, ↓). Application of equation (2) to the spectra shown in figure 11(c) results in $P = 0.08$ ($P = 0.05$) at the peak position of the majority (minority) part of the surface state. The spin polarization of the sample can be estimated by

$$P_{Gd} = P/P_{tip} \cos\Theta \tag{3}$$

where P_{tip} is the spin polarization of the tip and Θ is the angle between the magnetization directions of the tip and the sample. Assuming a constant spin polarization of the tip

† If the exchange splitting Δ_{ex} is too large one spin component would be too far from the Fermi level and not accessible by STS, as e.g. in the case of Fe(001), where Δ_{ex} amounts to 2.1 eV and only the minority band appears as a peak in the $\mathrm{d}I/\mathrm{d}U$-spectra just above the Fermi level [33].

‡ Later we will show in the discussion of figure 13 that this assumption is justified by our experimental results.

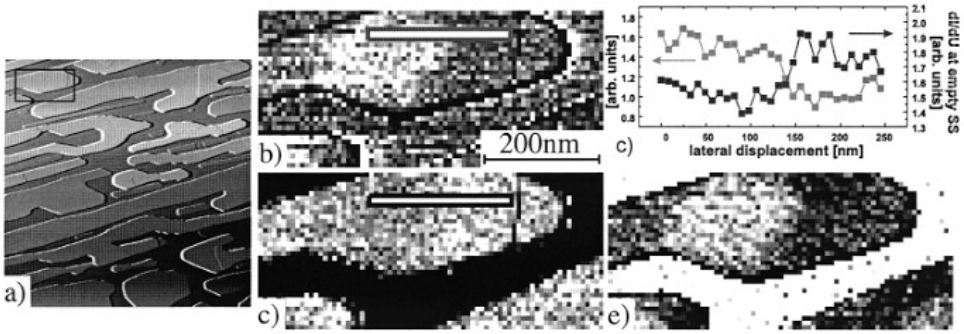

Figure 12. (a) Topography of 10 ML Gd grown on W(110) with the substrate held at 530 K. (b) In the $\mathrm{d}I/\mathrm{d}U$-image measured at $U = -0.2$ V the left part of the island is brighter than the right part indicating a parallel alignment of the filled surface state spin part with the tip spin polarization at the Fermi level. (c) $\mathrm{d}I/\mathrm{d}U$-image measured at $U = +0.45$ V. (d) Plot of the $\mathrm{d}I/\mathrm{d}U$-signal drawn along the line sections indicated above. (e) Asymmetry image (linear scale bar: 23%) calculated from (a) and (b).

$S = 0.44$ [6] we obtain $P \approx 0.20$ (-0.12) for the majority (minority) part of the surface state, which is about a factor of two below the results of spin-resolved (inverse) PES data [11, 12]. One possible reason for this difference is a non-collinear magnetic orientation between the tip and the sample, i.e. $\cos\Theta < 1$. While it is well known that the easy magnetization axis of Gd islands as used for this experiment (inset of figure 11(c)) lies preferentially within the plane [36, 37] the shape anisotropy of the magnetically coated tip should result in a considerable component perpendicular to the surface of the sample.

3.3. Imaging of magnetic domains

The high spatial resolution down to the atomic scale is the special merit of scanning tunnelling microscopy and spectroscopy. We performed spatially resolved measurements at $T = 70$ K with a W tip coated with 5–10 ML Fe on a sample prepared by depositing 10 ML of Gd on the W(110) substrate held at 530 K. This preparation procedure leads to partially coalesced Gd islands ($\Theta_{\mathrm{loc}} \approx 20$ ML) with a Gd wetting layer on the W(110) substrate as shown in the STM image of figure 12(a). Figures 12(b) and (c) show $\mathrm{d}I/\mathrm{d}U$-images at $U = -0.2$ V and $U = +0.45$ V, i.e. sample biases which correspond to filled and empty parts of the surface state, respectively, measured within the box of figure 12(a). Both images show a domain wall crossing the island from top to bottom. A closer inspection of line sections drawn along the grey and black box from left to right across this domain wall reveals that both the filled and the empty surface state spin parts increase and decrease in intensity on a lateral scale below 20 nm, respectively. The contrast between these two domains was one of the highest ever observed pointing to the fact that the magnetization of the tip is more or less in line with the magnetization of the sample.

Figure 13(a) shows tunnelling $\mathrm{d}I/\mathrm{d}U$-spectra measured above these domains. The asymmetry with respect to the differential tunnelling conductivity $\mathrm{d}I/\mathrm{d}U$ at the surface state peak positions is obvious. The importance of an exchange-split surface state for a reliable demonstration of spin polarized tunnelling might be illustrated by the comparision with tunnelling spectra measured above a similar sample but using a pure W tip (inset of figure 13(a)). Even in the latter case we could find spectra that exhibit significant variations in the $\mathrm{d}I/\mathrm{d}U$-signal at both spin parts of the surface state. However, these

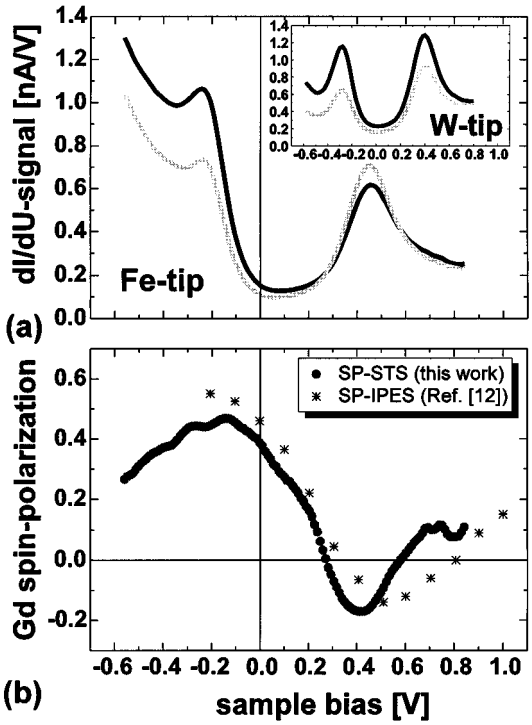

Figure 13. (a) Tunnelling spectra as measured with an Fe-covered probe tip above adjacent domains. An asymmetry of the $\mathrm{d}I/\mathrm{d}U$-signal between the empty and filled part of the surface state can clearly be recognized. In contrast, variations in the $\mathrm{d}I/\mathrm{d}U$-signal when measured with a pure W tip are always symmetric (inset). (b) Spin polarization of the tunnelling current between an Fe-covered probe tip and the Gd(0001) surface at $T = 70$ K (●) compared to spin-polarized inverse photoemission data of Gd(0001) measured at $t = 130$ K (∗) by Donath *et al* [12].

variations are symmetric, i.e. both spin parts are simultaneously diminished or enhanced. The spin polarization of the sample can be estimated by applying equations (2) and (3) whereby in this case $\mathrm{d}I/\mathrm{d}U_{\uparrow(\downarrow)}(U)$ is the intensity of the $\mathrm{d}I/\mathrm{d}U$-signal measured above adjacent magnetic domains. The result is shown in figure 13(b). The polarization exhibits extreme values at $U = -0.13$ V and $U = +0.42$ V, i.e. at bias voltages just below the peak positions of the surface state. For comparison we have included values of the spin polarization of homogeneous, approximately 30 ML thick Gd(0001) films grown on W(110) as determined by means of spin-resolved inverse photoemission spectroscopy (SP-IPE) [12]. An excellent overall agreement can be recognized†. Both SP-STS as well as SP-IPE data exhibit a positive spin polarization P_{Gd} on both sides of the Fermi level. In more detail, P_{Gd} amounts to about 0.5 close to the position of the majority surface state, decreases to $P_{\mathrm{Gd}} \approx 0.4$ at the Fermi level and vanishes about 300 meV above the the Fermi level. With both experimental techniques a negative spin polarization can only be recognized around the peak position of the minority surface state, while the spin polarization turns to positive values again for unoccupied electronic states being energetically further apart from the Fermi level.

† This agreement indicates that in this particular case the term $\cos\Theta \approx 1$ (cf equation (3)), i.e. the magnetization directions of the tip and the sample are more or less collinear. Indeed, it has been proposed that the easy magnetization direction of Gd/W(110) at low temperatures and thickness is out of plane [39].

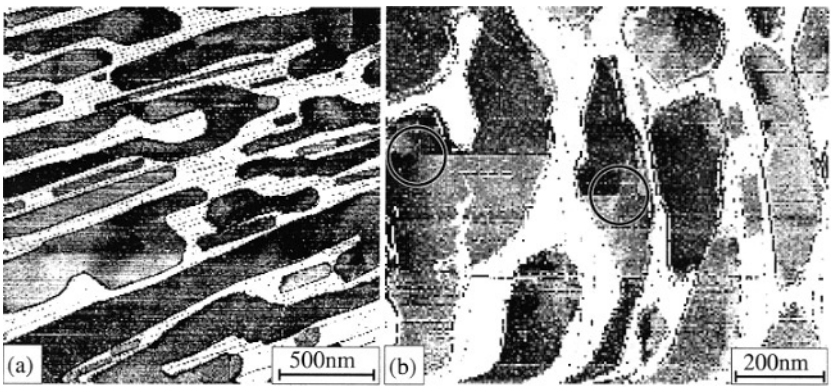

Figure 14. Asymmetry images of Gd(0001) islands on W(110) as measured with W tips coated by (a) 5–10 ML Fe and (b) 100–200 ML Fe. Due to the stronger stray field of the latter tip the magnetization of individual islands is accidentally switched twice (circles).

Figure 14 shows asymmetry images of Gd films with a topography similar to figure 12 as measured with W tips coated by 5–10 ML Fe (a) and 100–200 ML Fe (b). We never observed any indication of tip-induced changes of the sample domain structure for Fe coatings with $\Theta_{tip} \leqslant 10$ ML. If, however, $\Theta_{tip} \geqslant 100$ ML tip-induced magnetic modifications were observed (figure 14(b)). The sample was scanned from bottom to top with a tip coated with an Fe film of 100–200 ML thickness. Two circles indicate locations where a checkerboard pattern was observed which is characteristic for a magnetization reversal of single Gd islands. Magnetic switching of the tip can be ruled out since other Gd islands are imaged unchanged in subsequent scan lines.

4. Summary

In summary, we have presented results that illustrate the progress recently made in the field of magnetically sensitive scanning probe methods. In particular, magnetic force microscopy has been used to study the spin reorientation transition of thin Co films on Au(111) under UHV conditions. The sensitivity and spatial resolution of this technique have been demonstrated by imaging of domains of Co films as thin as 1.8 ML and details of domain walls, respectively. We have realized spin-polarized STM by tunnelling between a magnetically coated thin film tip and a sample which exhibits an exchange-split surface state, i.e. Gd(0001). We showed that the bias-dependent spin polarization of the tunnelling current is in excellent agreement with earlier experiments performed by means of spin-resolved inverse photoelectron spectroscopy. Magnetic domains of Gd(0001) films grown on W(110) were imaged non-destructively using W tips coated with Fe films of 5–10 ML and a spatial resolution below 20 nm was demonstrated.

References

[1] Binning G and Rohrer H 1987 *Rev. Mod. Phys.* **59** 615
[2] Wiesendanger R 1994 *Scanning Probe Miroscopy and Spectroscopy: Methods and Applications* (Cambridge: Cambridge University Press)
[3] Újfalussy B, Szunyogh L, Bruno P and Weinberger P 1996 *Phys. Rev. Lett.* **77** 1805
[4] Slonczewski J C 1989 *Phys. Rev.* B **39** 6995

[5] Tedrow P M, Meservey R and Fulde P 1970 *Phys. Rev. Lett.* **25** 1270
[6] Tedrow P M and Meservey R 1973 *Phys. Rev.* B **7** 318
[7] Julliere M 1975 *Phys. Lett.* A **54** 225
[8] Prinz G 1995 *Phys. Today* **58** 24
[9] Wiesendanger R, Güntherodt H J, Güntherodt G, Gambino R J and Ruf R 1990 *Phys. Rev. Lett.* **65** 247
[10] Wiesendanger R, Shvets I V, Bürgler D, Tarrach G, Güntherodt H J, Coey J M D and Gräser S 1992 *Science* **255** 583
[11] Li D, Pearson J, Bader S D, McIlroy D N, Waldfried D and Dowben P A 1995 *Phys. Rev.* B **51** 13 895
[12] Donath M, Gubanka B and Passek F 1996 *Phys. Rev. Lett.* **77** 5138
[13] Allenspach R, Spamanoni M and Bischof A 1990 *Phys. Rev. Lett.* **65** 3344
[14] Speckmann M, Oepen H P and Ibach H 1995 *Phys. Rev. Lett.* **75** 2035
[15] Dreyer M, Kleiber M, Wadas A and Wiesendanger R 1999 *Phys. Rev.* B **59** 4273
[16] Albrecht T R, Grütter P, Horne D and Rugar D 1991 *J. Appl. Phys.* **69** 668
[17] Wadas A, Dreyer M, Löhndorf and Wiesendanger R 1997 *Appl. Phys.* A **64** 353
[18] Barth J V, Brune H, Ertl G and Behm R J 1990 *Phys. Rev.* B **42** 9307
[19] Voigtländer B, Meyer G and Amer N M 1991 *Phys. Rev.* B **44** 10 354
[20] Huber E E, Smith D O and Goodenough J B 1958 *J. Appl. Phys.* **3** 294
[21] Löhndorf M, Wadas A and Wiesendanger R 1997 *Appl. Phys.* A **65** 511
[22] Dietze H D and Thomas H 1961 *Z. Phys.* **163** 523
[23] Hope S, Gu E, Choi B and Bland J A C 1998 *Phys. Rev. Lett.* **80** 1750
[24] Wu R, Li C, Freeman A J and Fu C L 1991 *Phys. Rev.* B **44** 9400
[25] Li D, Hutchings C W, Dowben P A, Hwang C, Wu R T, Onellion M, Andrews A B and Erskine J L 1991 *J. Magn. Magn. Mater.* **99** 85
[26] Li D, Dowben P A, Ortega J E and Himpsel F J 1994 *Phys. Rev.* B **49** 7734
[27] Mulhollan G A, Garrison K and Erskine J L 1992 *Phys. Rev. Lett.* **69** 3240
[28] Starke K, Navas E, Baumgarten L and Kaindl G 1993 *Phys. Rev.* B **48** 1329
[29] Weschke E, Schüssler-Langeheine C, Meier R, Fedorov A V, Starke K, Hübinger F and Kaindl G 1997 *Phys. Rev. Lett.* **77** 3415
[30] Pascal R, Zarnitz Ch, Bode M, Getzlaff M and Wiesendanger R 1997 *Appl. Phys.* A **65** 603
[31] Getzlaff M, Bode M and Wiesendanger R 1998 *Surf. Sci.* **410** 189
[32] Getzlaff M, Bode M, Heinze S, Pascal R and Wiesendanger R 1998 *J. Magn. Magn. Mater.* **184** 155
[33] Stroscio J A, Pierce D T, Davies A, Celotta R J and Weinert M 1995 *Phys. Rev. Lett.* **75** 2960
[34] Bode M, Getzlaff M and Wiesendanger R 1998 *Phys. Rev. Lett.* **81** 4256
[35] Wu R and Freeman A J 1992 *Phys. Rev. Lett.* **69** 2867
[36] Farle M and Lewis W A 1994 *J. Appl. Phys.* **75** 5604
[37] Fedorov A V, Valla T, Huang D J, Reisfeld G, Loeb F, Liu F and Johnson P D 1998 *J. Electron. Spectrosc. Relat. Phenom.* **92** 19
[38] Bode M, Getzlaff M and Wiesendanger R 1999 *J. Vac. Sci. Technol.* A at press
[39] André G, Aspelmeier A, Schulz B, Farle M and Baberschke K 1995 *Surf. Sci.* **326** 275